

# Uncertainty quantification for improving radiomic-based models in radiation pneumonitis prediction.

Chanon Puttanawat1,2,\* Romen Samuel Wabina2, Nat Sirirutbunkajorn3,\*

1. *Chakri Naruebodindra Medical Institute, Faculty of Medicine, Ramathibodi Hospital, Mahidol University, Samut Prakan, Thailand*
2. *Department of Clinical Epidemiology and Biostatistics, Faculty of Medicine, Ramathibodi Hospital, Mahidol University, Bangkok, Thailand*
3. *Department of Diagnostic and Therapeutic Radiology, Faculty of Medicine, Ramathibodi Hospital, Mahidol University, Bangkok, Thailand*

*\*Corresponding authors*

*Nat Sirirutbunkajorn E-mail: nat19012537@gmail.com*

*Chanon Puttanawat E-mail: chanonp@protonmail.com*

## Abstract

**Background and Objective:** Radiation pneumonitis (RP) is a side effect of thoracic radiation therapy. Recently, Machine learning (ML) models enhanced with radiomic and dosiomic features provide better predictions by incorporating spatial information beyond DVHs. However, to improve the clinical decision process, we propose to use uncertainty quantification (UQ) to improve the confidence in model prediction. This study evaluates the impact of post hoc UQ methods on the discriminative performance and calibration of ML models for RP prediction.

**Methods:** This study evaluated four ML models: logistic regression (LR), support vector machines (SVM), extreme gradient boosting (XGB), and random forest (RF), using radiomic, dosiomic, and dosimetric features to predict RP. We applied UQ methods, including Platt scaling, isotonic regression, Venn-ABERS predictor, and Conformal Prediction, to quantify uncertainty. Model performance was assessed through Area Under the Receiver Operating Characteristic curve (AUROC), Area Under the Precision-Recall Curve (AUPRC), and Adaptive Calibration Error (ACE) using Leave-One-Out Cross-Validation (LOO-CV).

**Results:** UQ methods enhanced predictive performance, particularly for high-certainty predictions, while also improving calibration. Radiomic and dosiomic features increased model accuracy but introduced calibration challenges, especially for non-linear models like XGB and RF. Performance gains from UQ methods were most noticeable at higher certainty thresholds.

**Conclusion:** Integrating UQ into ML models with radiomic and dosiomic features improves both predictive accuracy and calibration, supporting more reliable clinical decision-making. The findings emphasize the value of UQ methods in enhancing applicability of predictive models for RP in healthcare settings.

**KEYWORDS:** Uncertainty quantification, Calibration, Machine learning, Radiomic, Radiation pneumonitis, Esophageal cancer

## 1. Introduction

Radiation pneumonitis (RP) is a common side effect of thoracic radiation therapy, characterized by inflammation of the lungs resulting from radiation exposure. The timing and severity of RP can vary widely among patients, but it is typically detected within the first 8 months after radiation [1]. The incidence rate ranges from 15–40% among patients receiving thoracic radiation [2].

In recent years, machine learning (ML), a subfield of artificial intelligence (AI), has been increasingly used to develop predictive models for RP. ML models typically rely on traditional features, such as those derived from dose-volume histograms (DVHs) or clinical data [2]. However, DVH-based features lack spatial information about the radiation dose distribution. To address this limitation, spatially informed quantitative features known as radiomics (or dosiomics when derived from dose distributions) have been developed. Previous studies have shown that incorporating dosiomic and/or radiomic features can significantly enhance the predictive performance of models based solely on DVHs or clinical features [3–6].

From previous studies, ML models with radiomics and/or dosiomics are commonly evaluated based on their discriminative ability. However, high discriminative performance alone is insufficient for clinical applications since it does not guarantee robustness, generalizability across diverse patient populations, or practical integration into clinical workflows. In the medical field, inaccurate or overly confident predictions can lead to harmful consequences, such as misdiagnosis, inappropriate treatment decisions, or delayed interventions that compromise patient safety and outcomes. For general classification model, we can view probability output as uncertainty estimate. However, a model might have good discriminative ability but exhibit inaccurate confidence levels [7–9]. This is where uncertainty quantification (UQ) plays a crucial role. UQ helps assess not only whether a model is correct but also how certain of the model is in its predictions, thereby promoting reliable and more trustworthy application of AI in healthcare setting [10–13]. Furthermore, previous studies also show that incorporating UQ methods can help improve model discriminative performance and clinical decision support in various ML in medical task such as Alzheimer's disease prediction [14], diabetic retinopathy detection [15] and polyp classification [16].

A recent review of UQ in radiotherapy identified its applications in image synthesis, registration, contouring, dose prediction, and outcome prediction [17]. For outcome prediction, UQ has been applied to tasks like local control prediction [18], survival prediction [19] and locoregional recurrence prediction [20]. For RP prediction, existing studies [21,18] have focused on improving uncertainty evaluation metrics but have not explicitly demonstrated how uncertainty enhances discriminative performance.

In this study, we aim to explore the impact of integrating UQ into widely used ML models that leverage radiomic and dosiomic features for RP prediction in esophageal cancer patients. While prior studies have employed Bayesian networks [21] and Gaussian processes

integrated with deep neural networks [18] for UQ in RP prediction, these methods require integration into the model during training. This requirement renders them unsuitable for existing ML models, highlighting the need for alternative methods that can seamlessly retrofit UQ capabilities into pre-existing frameworks. Our focus will be on post hoc (adjustment occur after initial model training) UQ methods since it can easily be integrated into the existing common radiomic based ML model in RP without requiring extensive modifications. Additionally, we evaluate the models using both discriminative and uncertainty evaluation metrics, and we assess how incorporating uncertainty can enhance discriminative performance.

## 2. Materials and Methods

### 2.1 Dataset

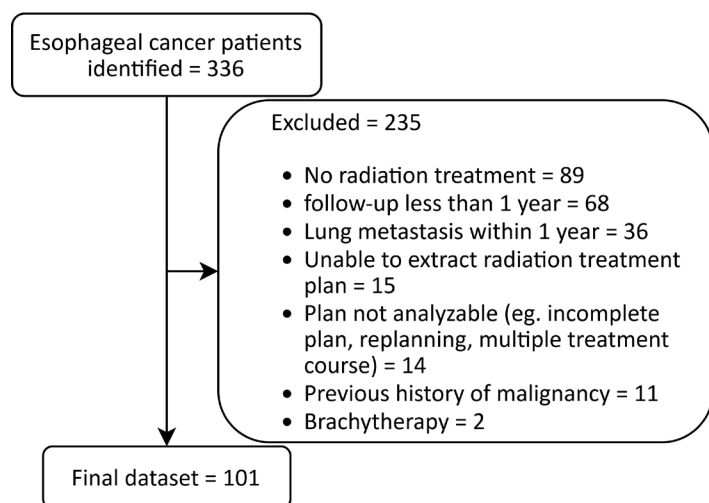


**Figure 1:** Consort Diagram

This study was approved by Institutional Review Board (IRB) of Ramathibodi hospital, Bangkok, Thailand approval (MURA2024/933) in accordance with the Declaration of Helsinki. This study included esophageal cancer patients aged over 15 years who underwent thoracic radiation therapy for esophageal cancer, regardless of the indication (pre-operative concurrent chemoradiation, definitive chemoradiation, post-op radiation or palliative radiation) between January 2011 and June 2019. Patients were excluded if they lacked treatment planning data, had a history of malignancy or prior radiation therapy, had underlying interstitial lung disease, had a follow-up period of less than one year, developed lung metastases within a year, or were treated with brachytherapy. A radiation oncologist reviewed and extracted clinical data for each patient from electronic medical records. National Cancer Institute Common Terminology Criteria for Adverse Events version 5.0 (CTCAE v5.0) was used as the basis for grading radiation pneumonitis. Patients with no symptoms or radiographic features were defined as grade 0. Patients with mild symptoms not requiring steroids or with radiographic features only were defined as grade 1. Patients with symptoms interfering with daily activities or patients requiring steroids were defined as grade 2. Patients requiring steroid and oxygen were defined as grade 3

and patients requiring intubation were defined as grade 4. For this study, positive class was defined as grade 1 or more radiation pneumonitis.

Initially, 336 esophageal cancer patients were identified, but 235 were excluded primarily due to the absence of radiation therapy or loss follow-up. Ultimately, 101 patients were eligible and included in the final analysis (**Figure 1**). Patient characteristics are summarized in **Table 1** and treatment characteristics are summarized in **Table 2**.

**Table 1:** Patient characteristics (N=101)

Parameters	Median (Range)/N (%)
Age	61 (26-93)
<b>Gender</b>	
Male	89 (88%)
Female	12 (12%)
<b>Smoking status</b>	
Never	29 (29%)
Active	25 (25%)
Quit smoking < 10 years	33 (33%)
Quit smoking > 10 years	14 (13%)
<b>ECOG performance status</b>	
0	32 (32%)
1	60 (60%)
2	9 (8%)
<b>Stage</b>	
1	4 (4%)
2	3 (3%)
3	71 (70%)
4	23 (23%)
<b>Chemotherapy regimen</b>	
Cisplatin + 5-FU	23 (23%)
Carboplatin + 5-FU	8 (8%)
Carboplatin + paclitaxel	60 (59%)
Carboplatin alone	2 (2%)
Paclitaxel alone	2 (2%)
No chemotherapy	6 (6%)

**Table 2:** Treatment characteristics (N=101)

Parameters	Median (Range)/N (%)
<b>Surgery</b>	
Yes	26 (26%)
No	75 (74%)
Prescription dose	50.4 (30.0-60.0)
Prescription dose per fraction	1.8 (1.8-3.0)
<b>RT technique</b>	

3D conformal	78 (77%)
IMRT/VMAT	9 (9%)
Combine	14 (14%)
<b>RT setting</b>	
Preoperative	47 (47%)
Postoperative	1 (1%)
Definitive	49 (48%)
Palliative	4 (4%)
<b>RP grade</b>	
0	38 (38%)
1	58 (57%)
2	5 (5%)
3	0 (0%)
<b>Dosimetric Parameter (Lung)</b>	<b>Mean (Range)</b>
MLD (Gy)	10.3 Gy (1.1-16.3 Gy)
V5 (%)	48.9% (3.4-74.0%)
V10 (%)	32.0% (2.8-53.0%)
V20 (%)	16.2 (2.1-31.5%)
V30 (%)	11.1 (1.6-26.0%)
V40 (%)	6.2% (0.0-18.9%)

## 2.2 Preprocessing and Features

The preprocessing and feature extraction steps are similar to those used in our previous research [3,22]. The total dose distribution was converted to an equivalent dose of 2 Gy (EQD2) using the following formula:  $EQD2_k = \sum_i^N \frac{d_{i,k} + d_{i,k}^2 / (\alpha/\beta)}{1 + 2/(\alpha/\beta)}$ , where  $d_{i,k}$  is dose at fraction  $i$  and voxel  $k$ . The value of  $\alpha/\beta$  was set to 3. From now on the dose distribution will refer to dose distribution in EQD2. The dose distributions and pretreatment CT images were then resampled to have voxel size of  $1.5 \times 1.5 \times 1.5$  mm<sup>3</sup> using b-spline algorithm. The regions of interests (ROIs) were resampled to match the pretreatment CT images using the nearest neighbor algorithm.

In this study, we extracted two types of features, dose-based (dosimetric and dosiomic) features and features based on pretreatment CT image (radiomic features). Dosimetric features, including mean lung dose, generalized equivalent uniform dose, and relative lung volume dose greater than  $x$  Gy ( $V_x$ ), for  $x$  in [5, 10, ..., 70], were extracted. Dosiomic features were calculated from dose distribution in lung ROIs using the Pyradiomics library, encompassing first-order statistics (18 features) and texture features based on gray-level cooccurrence matrix (GLCM) (24 features), gray-level run length matrix (GLRLM) (16 features), gray-level size zone matrices (GLSZM) (16 features) and neighborhood gray tone difference matrices (NGTDM) (5 features), in total of 61 texture features. Radiomic features were extracted from pretreatment CT images of three lung ROIs defined by different radiation dose thresholds (10 Gy, 15 Gy, and 20

Gy). The features description is the same as dosiomic features but the number of radiomic features are 3 times dosiomic features due to the extraction from three distinct ROIs.

All features (dosimetric, dosiomic, and radiomic) then were standardized to a scale of 0 to 1. In total, each patient comprised of 15 dosimetric, 61 dosiomic, and 183 radiomic features. To reduce redundancy, Spearman's rank correlation test was employed to identify the correlation between all possible pairs of features. If a correlation exceeding 0.8 was identified, one of the features with the highest correlation to the rest of features was eliminated. After this process, each patient had 58 features (6 dosimetric, 37 dosiomic and 25 radiomic). No further feature selection was performed. Radiomic and dosiomic features were extracted in accordance with the Imaging Biomarker Standardization Initiative (IBSI) guidelines [23] to ensure methodological consistency and reproducibility. This process was implemented using PyRadiomics [24], an open-source Python library specifically designed for radiomic analysis.

### 2.3 Training process

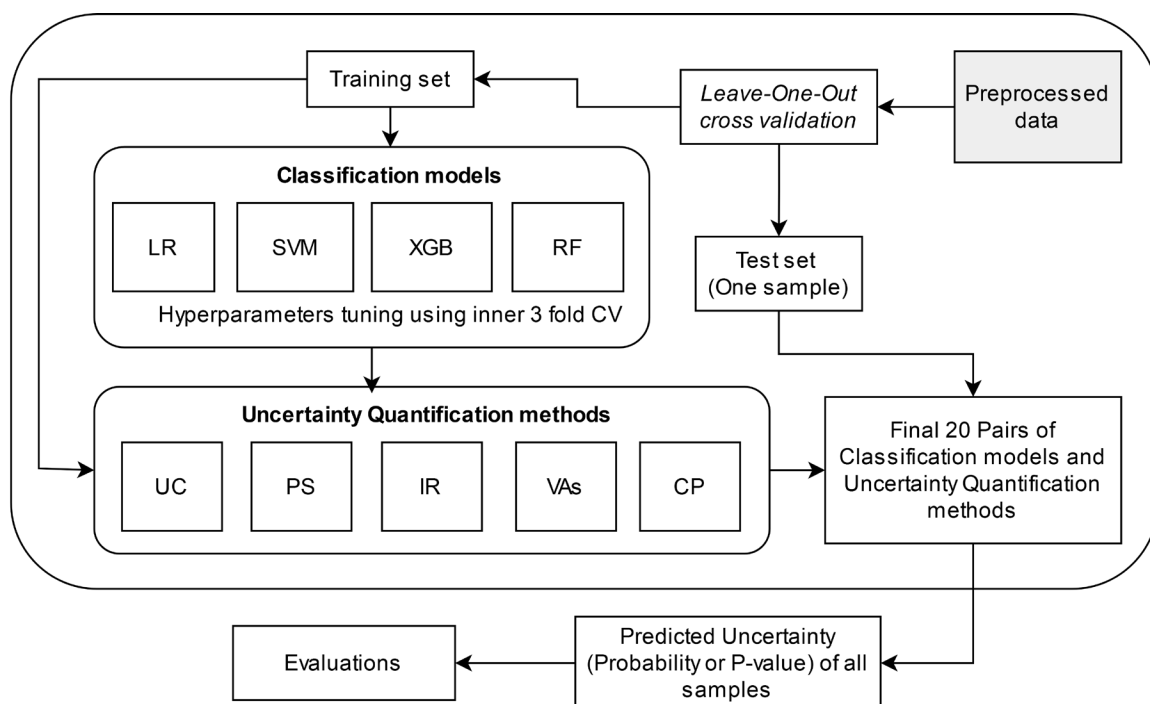


**Figure 2:** Training process

An overview of the training process is shown in **Figure 2**. The procedure starts with the preprocessed data, which is split into training and test sets. A Leave-One-Out (LOO-CV) approach is employed where a single data sample is held out as the test set while the remaining samples generate the training set to ensure that each sample is tested once. To address potential class imbalance, a weighted loss function was done using the built-in functionality of the machine learning libraries. Several models, including logistic regression (LR), support vector machines (SVM), extreme gradient boosting (XGB), and random forest (RF) were employed for the

classification task. These models undergo hyperparameter tuning using an inner three-fold nested cross-validation within the training set. Details of the tuned hyperparameters for each model can be found in **Supplementary Table 1**. Once the models are trained and tested, UQ methods were then applied using uncalibrated (UC), Platt scaling (PS) [25], isotonic regression (IR), VennABERS predictor (VAs) [26], or Conformal Prediction (CP) [27–29] as described in the next section. These methods were applied to the predictions to quantify the uncertainty associated with each prediction, either as probabilities (UC, PS, IR and VAs) or p-values (CP). The goal is to integrate each classification model with each UQ method to generate 20 pairs of models.

## 2.4 Uncertainty Quantification Methods

Given a dataset  $\{(x_1, y_1), \dots, (x_n, y_n)\}$ , where  $x_i$  represents the feature vector for the  $i^{th}$  instance and  $y_i$  represents the corresponding label, we focus on a binary classification problem. The uncertainty score, denoted as  $s(x)$ , is defined as:

$$s(x) = \begin{cases} 1 - p(x), & \hat{y} \text{ is positive} \\ p(x), & \hat{y} \text{ is negative} \end{cases}$$

Here,  $p(x)$  represents the predicted probability or p-value of the positive class, potentially with or without the application of UQ methods (raw output from classifier, denoted as  $f(x)$ ). This formulation assumes that a prediction  $\hat{y}$  is made based on a threshold of  $p(x) \geq 0.5$  ( $f(x) \geq 0.5$  if CP since CP output p-value). Consequently, the model exhibits the highest certainty when the predicted probability/p-value is either 0 or 1. Below are detailed descriptions of each uncertainty quantification method:

- UC: The UC method simply refers to using the output probabilities from the classifier without applying any UQ techniques. Thus,  $p(x)$ , is equivalent to  $f(x)$ .
- PS [25]: PS is a parametric calibration method that fits LR to the classifier's output scores, converting them into calibrated probabilities. The process starts by applying a classifier without UQ to obtain a dataset of output-label pairs  $\{(f(x_1), y_1), \dots, (f(x_m), y_m)\}$ , where  $f(x_i)$  represents the raw output score from the classifier, and  $y_i \in \{0,1\}$  is the corresponding true label in a binary classification. These output-label pairs are then used to fit a LR defined by:

$$p(x|f(x)) = \frac{1}{1 + \exp(a + bf(x))}$$

where  $a$  and  $b$  are learned parameters by minimizing the negative log-likelihood of the observed data. This method ensures that the predicted probabilities lie within the range  $[0, 1]$  and are more reliable for interpreting uncertainty.

- IR: IR is a non-parametric calibration technique that fits the data to a piecewise constant function, subject to the constraint that the function is non-decreasing. The optimization process involves minimizing the root mean square error IR is Optimized by minimizing the root mean square error between predicted probabilities  $p(x_i)$  and actual outcomes  $y_i$ .

- VAs [26]: VAs is a calibration technique based on Venn prediction, provides multiple probability estimates instead of a single probability by applying two IR models to the raw output of a classifier. It consists of two steps: first, IR is fitted to the probability of being a positive class using the training set  $\{(f(x_1), y_1), \dots, (f(x_m), y_m)\}$  along with a test sample  $(f(x_i), 1)$ . Second, IR is fitted to the probability of being a negative class using the training set  $\{(1 - f(x_1), y_1), \dots, (1 - f(x_m), y_m)\}$  along with a test sample  $(f(x_i), 0)$ . The first IR model computes  $p_1(x_i)$ , the probability of  $x_i$  belonging to class 1 given  $f(x_i)$  while the second IR model computes  $p_0(x_i)$ , the probability of  $x_i$  belonging to class 0 given  $f(x_i)$ . In practice, multiple probabilities will be merge to  $p(x)$  by:

$$p(x) = \frac{p_1}{1-p_0+p_1}.$$

- CP [27–29]: CP provides a framework for generating prediction sets for any model. It works by evaluating how well a new prediction aligns with the distribution of previously observed data, using insights learned from the training set. To compute p-value within CP framework, we first calculate the nonconformity score, denoted as  $\alpha_i$ , for a given data  $x_i$ . Nonconformity score  $\alpha_i$  is defined as  $-\log f(x_i)$  [14,30]. This score measures how "non-conforming" the test data is compared to the training data distribution. Once the nonconformity scores are obtained, they are used to compute the p-value,  $p(x)$ , which reflects how the test point is deviated relative to the training set. Specifically, the p-value is calculated as:

$$p(x_{m+1}) = \frac{|\{i=1, \dots, m+1: \alpha_i \geq \alpha_{m+1}\}|}{m+1} [31,32].$$

Where  $\{\alpha_1, \dots, \alpha_m\}$  represents the set of nonconformity score from the training dataset and  $\alpha_{m+1}$  is the nonconformity score of the test data.

## 2.5 Evaluations

Evaluation was performed on a test set that aggregates all test data from each fold of the LOO CV. To assess predictive performance, we calculated the Area Under the Receiver Operating Characteristic Curve (AUROC) and the Area Under the Precision-Recall Curve (AUPRC). Additionally, we evaluated the UQ methods using uncertainty evaluation metric, specifically a calibration metric, which can be viewed as a form of uncertainty evaluation. Calibration metrics assess the alignment between predicted probabilities and the actual frequency of correct predictions, providing insight into how well the model's predicted confidence reflects reality. We used the Adaptive Calibration Error (ACE) [33] as our calibration metric. Given number of classes ( $K$ ), number of samples ( $N$ ) and number of ranges ( $R$ ), ACE is defined as:

$$ACE = \frac{1}{KR} \sum_{k=1}^K \sum_{r=1}^R |acc(r, k) - conf(r, k)|$$

where  $acc(r, k)$  and  $conf(r, k)$  are the accuracy and confidence of adaptive calibration range  $r$  for class label  $k$ , respectively. The calibration range  $r$  is determined by the  $\lfloor N/R \rfloor^{\text{th}}$  index of the sorted

probability output. A lower ACE suggests a better match between the predicted probabilities and actual outcomes, indicating a well-calibrated model while high ACE represents a significant discrepancy between the model’s predicted probabilities and the actual outcomes.

### 3. Results

In this section, we present three types of results. First, we examine the impact of incorporating prediction uncertainty into the predictive evaluation. Second, we assess the model’s performance with and without the inclusion of radiomic features. Finally, we compare UQ methods using an uncertainty evaluation metric.

#### 3.1 Uncertainty effect on Prediction performance

To explore the impact of UQ methods, we focused on the performance metrics for the top  $k\%$  most certain predictions. Specifically, we calculated AUROC and AUPRC (**Figure 3**) progressively, starting from the top 10% of the most certain predictions, incrementally increasing up to 100% of the dataset. This approach enabled us to compute performance metrics at various **coverage levels**, defined as the proportion of the dataset used in the evaluation, ranging from 0.1 to 1. By comparing performance across these coverage levels, we gained insights into how UQ methods influence the model’s performance. The models analyzed in this section were trained using all feature types (dosimetric, dosiomic, and radiomic).

In general, UQ methods enhance predictive performance across models for the most certain predictions, though their impact diminishes as coverage increases (**Figure 3**). The LR model is an exception, where most UQ methods provide similar or slightly reduced performance. Among the methods evaluated, VAs consistently underperform. In contrast, other UQ methods, generally improve performance, particularly at higher certainty thresholds

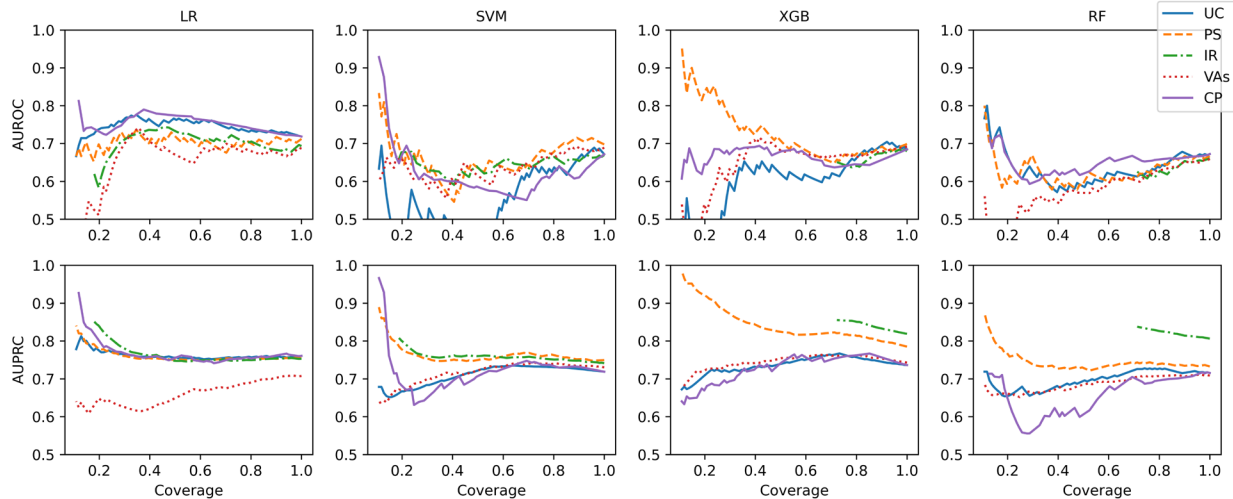


**Figure 3:** AUROC and AUPRC of each ML model with different UQ methods across varying coverage levels.

To better simulate clinical scenarios, where users assess output uncertainty before making decisions, we provided model performance metrics based on specific certainty thresholds in **Table 3**. Users may trust the model's predictions when the certainty is high and may be more skeptical when it is low. Specifically, we evaluated model performance at certainty thresholds of 0.5 (all data), 0.8, and 0.9. Predictions with certainty below these cutoffs were excluded from the evaluation.

The results in **Table 3** demonstrate that higher certainty thresholds reduce coverage. While UQ methods have minimal impact on performance without a cut point, they provide notable improvements at higher thresholds (such as 0.8 and 0.9). Focusing on cases where coverage exceeds 0.05, the highest AUROC is achieved by the LR model with the CP method (AUROC 0.78, AUPRC 0.76) at a cut point of 0.8. Similarly, the highest AUPRC is observed in the XGB model using the IR method (AUPRC 0.85, AUROC 0.64) at a cut point of 0.9. Overall, UQ methods not only improve performance but also increase coverage compared to the UC baseline

**Table 3:** This table presents AUROC and AUPRC for each classification model combined with UQ methods across different certainty thresholds (no threshold, 0.8 and 0.9). The baseline values for UC are shown, while changes for other UQ methods are expressed as increases (+) or decreases (−) relative to UC. (\*N/A indicates that no data were selected for evaluation at that threshold and improvements for UQ methods are calculated using 0 as the baseline)

Model	Uncertainty Method	No Cut point		Cut point 0.8			Cut point 0.9		
		AUROC	AUPRC	Coverage	AUROC	AUPRC	Coverage	AUROC	AUPRC
LR	UC	0.72	0.76	0.08	0.62	0.75	0.03	0.0	0.17
	PS	-0.01	-0.01	+0.35	+0.07	0.0	+0.18	+0.68	+0.61
	IR	-0.03	-0.01	+0.47	+0.1	-0.01	+0.18	+0.61	+0.66
	VAs	-0.03	-0.05	+0.32	+0.08	-0.13	+0.04	+0.25	+0.47
	CP	0.0	0.0	+0.27	+0.15	+0.01	+0.2	+0.72	+0.62
SVM	UC	0.67	0.72	0.13	0.62	0.66	0.0	N/A*	N/A*
	PS	+0.03	+0.03	+0.34	+0.01	+0.09	+0.24	+0.64*	+0.77*
	IR	-0.0	+0.02	+0.49	+0.04	+0.09	+0.19	+0.66*	+0.81*
	VAs	+0.02	+0.01	+0.3	-0.01	+0.05	+0.17	+0.64*	+0.67*
	CP	0.0	0.0	+0.09	+0.08	+0.01	+0.17	+0.69*	+0.71*
XGB	UC	0.68	0.74	0.44	0.64	0.73	0.22	0.28	0.72
	PS	+0.01	+0.05	+0.29	+0.01	+0.09	+0.44	+0.39	+0.1
	IR	-0.0	+0.08	+0.38	-0.0	+0.12	+0.53	+0.37	+0.13

	VAs	+0.01	+0.01	+0.18	+0.03	+0.03	+0.25	+0.42	+0.03
	CP	0.0	0.0	-0.23	0.0	-0.05	-0.12	+0.25	-0.07
RF	UC	0.67	0.72	0.16	0.73	0.67	0.03	1.0	1.0
	PS	-0.01	+0.02	+0.55	-0.12	+0.07	+0.46	-0.41	-0.27
	IR	-0.01	+0.09	+0.7	-0.09	+0.15	+0.76	-0.38	-0.17
	VAs	-0.01	-0.01	+0.48	-0.12	+0.02	+0.38	-0.46	-0.32
	CP	0.0	0.0	+0.03	-0.05	0.0	+0.05	-0.4	-0.28

### 3.2 Radiomic effect on predictive model

We evaluated the impact of radiomic and dosiomic features on model performance by training three versions of the models: (1) combining radiomic and dose-based features (dosiomic + dosimetric), (2) using only dose-based features, and (3) using only dosimetric features (**Figure 4**). For discriminative performance, we calculated AUROC and AUPRC, while ACE was used to assess calibration.

The results in **Figure 4** indicate that incorporating spatial features generally improved the model's discriminative ability, except for RF model, where the addition of both radiomic and dosiomic features slightly reduced performance, particularly in AUPRC. In terms of calibration, the LR model benefited from improved calibration with lower ACE, while other models exhibited higher ACE values, indicating a decline in calibration performance especially in RF (**Figure 4**). These findings suggest that while spatial features enhance predictive power, they may introduce calibration challenges, particularly for non-linear models.

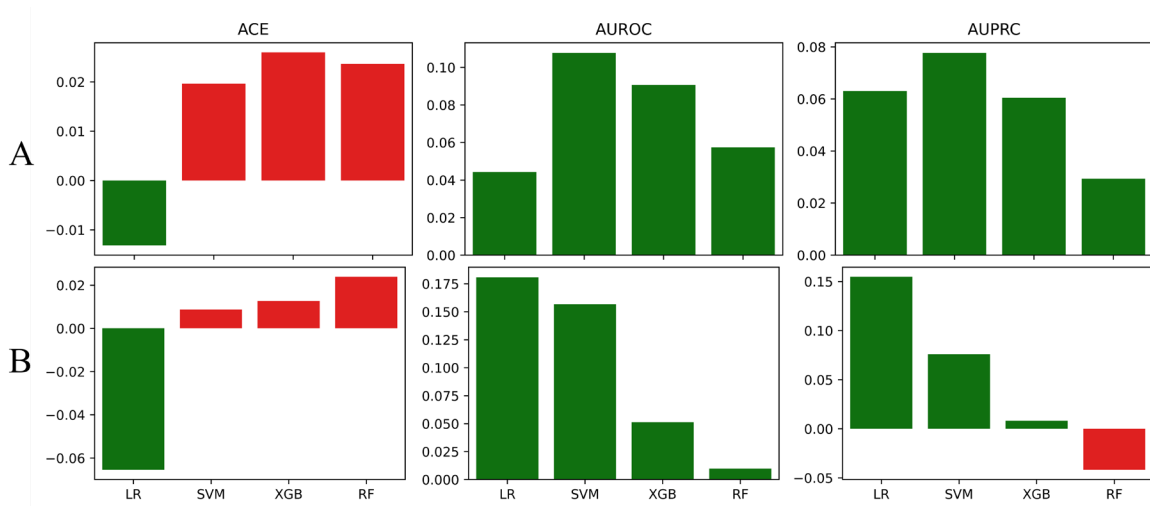


**Figure 4:** Differences in performance metrics between models using (A) radiomic and dose-based features compared to only dose-based features, and (B) radiomic and dose-based features compared to only dosimetric features.

compared to only dosimetric features. Green bars indicate performance improvement, while red bars indicate a decline in performance.

### 3.3 Effect of uncertainty quantification on calibration metrics

In this section, we evaluated the impact of UQ methods on the calibration metrics using ACE. We compare the ACE values before and after applying three calibration methods: Platt Scaling (PS), Isotonic Regression (IR), and Venn-ABERS predictor (VAs). CP is not included in this analysis since it outputs p-values, which are not applicable for ACE evaluation. The results indicate that all calibration methods improve ACE across the models (**Figure 5**). Specifically, the negative ACE values after calibration suggest a reduction in calibration error.

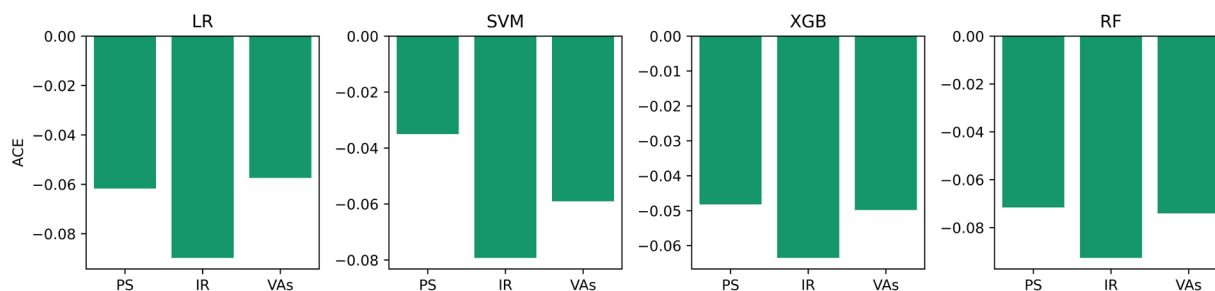


**Figure 5:** Difference of ACE between uncalibrated models compared with each model and uncertainty which gives probability output method. The green color indicates improving, else red.

The calibration plots provide a detailed comparison of the calibration performance of various classifiers under different UQ methods (**Figure 6**). The dotted diagonal line represents a perfectly calibrated model where predicted probabilities match observed outcomes. LR demonstrates the closest adherence to the perfect calibration line across all UQ methods, particularly with IR and PS but shows overconfidence under UC for high-probability predictions. Meanwhile, SVM, XGB, and RF exhibit significant calibration challenges, especially under the UC baseline where they tend to produce overconfident probability estimates. In terms of UQ methods, both IR and PS improve calibration, but the extent of improvement varies by model. However, VAs introduce instability in calibration that leads to erratic behavior across non-linear models, especially for RF, which demonstrates the poorest calibration overall.

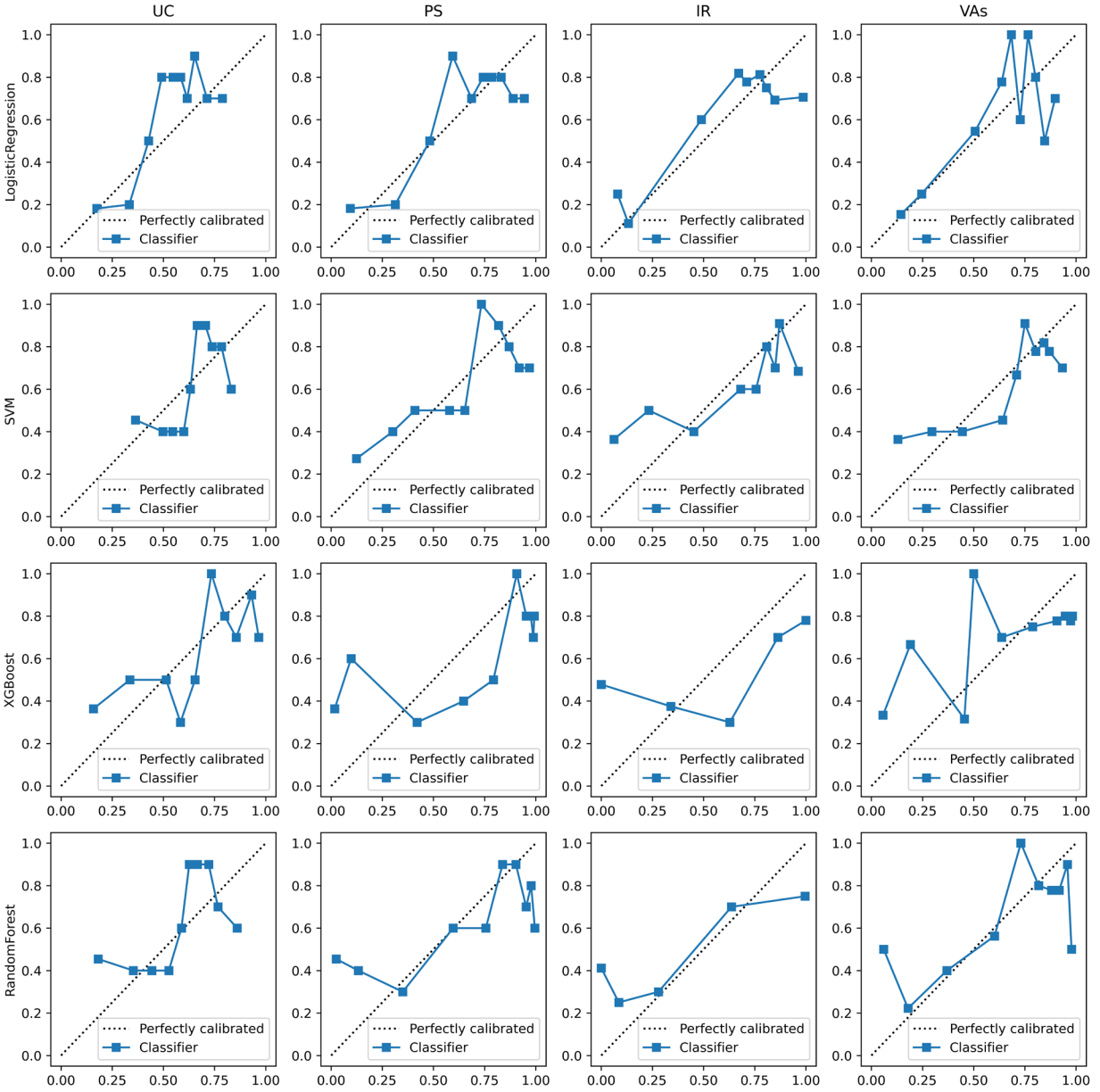


**Figure 6:** Calibration plot.

#### 4. Discussions

In this study, we investigated the impact of UQ on the performance of ML models for radiation RP prediction by employing several UQ methods, to assess the reliability of risk prediction, which are rarely assessed for clinical prediction models [34]. We applied four UQ methods, including PS, IS, VARs, and CP, across four prediction models, such as LR, SVM, XGB, and RF, and compared its resulting risk predictions to uncalibrated raw probabilities as baseline. According to a recent systematic review of radiomic- and dosiomic-based ML models for RP prediction [6], LR, SVM, and RF are among the most commonly used models in the

literature. Therefore, we selected these models to ensure that our findings are applicable to widely adopted approaches. The software code for this study is freely available at <https://github.com/44REAM/RP-Radiomic-Uncertainty>.

Our results demonstrate that UQ can enhance certainty estimation, as discriminative performance improves when the model is confident, except for the LR model which is known for its inherent well-calibrated nature [14,35] (**Figure 3 and Table 3**). UQ methods enhance AUROC and AUPRC for the most certain predictions since they prioritize areas where the model is confident by excluding uncertain predictions that may introduce errors or noise. UQ methods operate under the premise that uncertainty correlates with error. By ranking predictions based on certainty, they exploit this correlation to identify and prioritize regions where the model is most likely to be correct. However, as coverage grows, this correlation weakens because uncertainty measures may not perfectly capture all sources of error, such as systematic biases or unrepresented data distributions. Moreover, as coverage increases, the inclusion of uncertain predictions introduces noise and amplifies model limitations. This observation aligns with prior findings in radiomics-based locoregional recurrence prediction for head and neck cancer [20], which showed that rejecting low-certainty samples improves overall model performance.

Calibration methods such as PS, IR, and VAs offer limited benefits in improving certainty estimates in LR (**Figure 3**). However, CP can enhance uncertainty estimation in LR, as reflected by improved discriminative performance in confident predictions (**Figure 3**), aligning with previous findings [14]. This improvement can be attributed to the simpler structure of LR that avoids overfitting and allows calibration techniques to refine probability estimates effectively. In contrast, SVM, RF, and XGB, which are more complex than LR, exhibited poor calibration, which could be improved through calibration techniques (**Figures 3 and 5**). This can be attributed to the fact that increased model complexity often introduces overfitting and unreliable probability estimates, resulting in worsened calibration performance [36]. For instance, SVM and XGB can exacerbate calibration issues by assigning overly confident probabilities to outliers or misclassified points, further skewing their output reliability. Meanwhile, calibration issues in RF arise due to its ensemble structure (bagging ensemble), which averages predictions from decision trees and produces unreliable probabilities, particularly near class boundaries [35]. This results in poor estimates as RF struggles to model the smooth transitions in probability distributions necessary for well-calibrated outputs. Additionally, prior research similarly reports poorer calibration in SVM, RF [35] and XGB [37] compared to LR.

Incorporating radiomic and/or dosiomic features, which are often high-dimensional and complex, improved discriminative performance but introduced calibration challenges (**Figure 4**). While these features capture complex spatial patterns that enhance the model's ability to predict RP, they also increase the model's complexity, making it more prone to overfitting [38]. As such, the calibration errors observed after introducing radiomic and/or dosiomic features (**Figure 4**) in our results can be attributed to overfitting issue [39], consistent with the challenges associated with increasing model complexity discussed earlier. As such, ML models incorporating these

features require careful consideration of calibration strategies to ensure reliable performance. Without appropriate calibration, even highly accurate models may produce misleading probabilities, decreasing their utility in clinical decision-making.

In summary, our findings indicate that for clinical use, UQ techniques should be applied especially to complex ML models, such as SVM, RF, and XGB, to enhance the reliability of their predictions. LR, a less complex model, often achieves comparable or superior performance [40,41] with greater reliability in probability estimates. Furthermore, the inclusion of radiomic and/or dosiomic features enhances the models' discriminative power for RP prediction. However, these complex features also introduce calibration challenges, as they increase model dimensionality and potential overfitting, particularly in non-linear models.

### **Declaration of Generative AI and AI-assisted technologies in the writing process**

During the preparation of this work the author(s) used ChatGPT in order to improve readability and language. After using this tool/service, the author(s) reviewed and edited the content as needed and take(s) full responsibility for the content of the publication

### **References**

- [1] Jain V, Berman A. Radiation Pneumonitis: Old Problem, New Tricks. *Cancers* 2018;10:222.
- [2] Rodrigues G, Lock M, D'Souza D, Yu E, Van Dyk J. Prediction of radiation pneumonitis by dose–volume histogram parameters in lung cancer—a systematic review. *Radiother Oncol* 2004;71:127–38.
- [3] Puttanawarut C, Sirirutbunkajorn N, Khachonkham S, Plattaranutaporn P, Wongsawat Y. Biological dosiomic features for the prediction of radiation pneumonitis in esophageal cancer patients. *Radiat Oncol* 2021;16:220.
- [4] Kraus KM, Oreshko M, Bernhardt D, Combs SE, Peeken JC. Dosiomics and radiomics to predict pneumonitis after thoracic stereotactic body radiotherapy and immune checkpoint inhibition. *Front Oncol* 2023;13:1124592.
- [5] Bourbonne V, Da-ano R, Jaouen V, Lucia F, Dissaux G, Bert J, et al. Radiomics analysis of 3D dose distributions to predict toxicity of radiotherapy for lung cancer. *Radiother Oncol* 2021;155:144–50.
- [6] Sheen H, Cho W, Kim C, Han MC, Kim H, Lee H, et al. Radiomics-based hybrid model for predicting radiation pneumonitis: A systematic review and meta-analysis. *Phys Med* 2024;123:103414.
- [7] Shalev G, Shalev G, Keshet J. A Baseline for Detecting Out-of-Distribution Examples in Image Captioning. *Proc. 30th ACM Int. Conf. Multimed.*, Lisboa Portugal: ACM; 2022, p. 4175–84.
- [8] Yu D, Li J, Deng L. Calibration of Confidence Measures in Speech Recognition. *IEEE Trans Audio Speech Lang Process* 2011;19:2461–73.
- [9] Amodei D, Olah C, Steinhardt J, Christiano P, Schulman J, Mané D. Concrete Problems in AI Safety 2016.
- [10] Lambert B, Forbes F, Doyle S, Dehaene H, Dojat M. Trustworthy clinical AI solutions: A unified review of uncertainty quantification in Deep Learning models for medical image analysis. *Artif Intell Med* 2024;150:102830.

- [11] Begoli E, Bhattacharya T, Kusnezov D. The need for uncertainty quantification in machine-assisted medical decision making. *Nat Mach Intell* 2019;1:20–3.
- [12] Challen R, Denny J, Pitt M, Gompels L, Edwards T, Tsaneva-Atanasova K. Artificial intelligence, bias and clinical safety. *BMJ Qual Saf* 2019;28:231–7.
- [13] Niraula D, Cui S, Pakela J, Wei L, Luo Y, Ten Haken RK, et al. Current status and future developments in predicting outcomes in radiation oncology. *Br J Radiol* 2022;95:20220239.
- [14] Pereira T, Cardoso S, Guerreiro M, Mendonça A, Madeira SC. Targeting the uncertainty of predictions at patient-level using an ensemble of classifiers coupled with calibration methods, Venn-ABERS, and Conformal Predictors: A case study in AD. *J Biomed Inform* 2020;101:103350.
- [15] Ayhan MS, Kühlewein L, Aliyeva G, Inhoffen W, Ziemssen F, Berens P. Expert-validated estimation of diagnostic uncertainty for deep neural networks in diabetic retinopathy detection. *Med Image Anal* 2020;64:101724.
- [16] Carneiro G, Zorron Cheng Tao Pu L, Singh R, Burt A. Deep learning uncertainty and confidence calibration for the five-class polyp classification from colonoscopy. *Med Image Anal* 2020;62:101653.
- [17] Wahid KA, Kaffey ZY, Farris DP, Humbert-Vidan L, Moreno AC, Rasmussen M, et al. Artificial intelligence uncertainty quantification in radiotherapy applications – A scoping review. *Radiother Oncol* 2024;201:110542.
- [18] Sun W, Niraula D, El Naqa I, Ten Haken RK, Dinov ID, Cuneo K, et al. Precision radiotherapy via information integration of expert human knowledge and AI recommendation to optimize clinical decision making. *Comput Methods Programs Biomed* 2022;221:106927.
- [19] Lin Z, Cai W, Hou W, Chen Y, Gao B, Mao R, et al. CT-Guided Survival Prediction of Esophageal Cancer. *IEEE J Biomed Health Inform* 2022;26:2660–9.
- [20] Wang K, Dohopolski M, Zhang Q, Sher D, Wang J. Towards reliable head and neck cancers locoregional recurrence prediction using delta-radiomics and learning with rejection option. *Med Phys* 2023;50:2212–23.
- [21] Lee S, Ybarra N, Jeyaseelan K, Faria S, Kopek N, Brisebois P, et al. Bayesian network ensemble as a multivariate strategy to predict radiation pneumonitis risk. *Med Phys* 2015;42:2421–30.
- [22] Puttanawarut C, Sirirutbunkajorn N, Tawong N, Jiarpinitnun C, Khachonkham S, Plattaranutaporn P, et al. Radiomic and Dosiomic Features for the Prediction of Radiation Pneumonitis Across Esophageal Cancer and Lung Cancer. *Front Oncol* 2022;12:768152.
- [23] Zwanenburg A, Vallières M, Abdalah MA, Aerts HJWL, Andrearczyk V, Apte A, et al. The Image Biomarker Standardization Initiative: Standardized Quantitative Radiomics for High-Throughput Image-based Phenotyping. *Radiology* 2020;295:328–38.
- [24] Van Griethuysen JJM, Fedorov A, Parmar C, Hosny A, Aucoin N, Narayan V, et al. Computational Radiomics System to Decode the Radiographic Phenotype. *Cancer Res* 2017;77:e104–7.
- [25] Zadrozny B, Elkan C. Transforming classifier scores into accurate multiclass probability estimates. *Proc. Eighth ACM SIGKDD Int. Conf. Knowl. Discov. Data Min.*, Edmonton Alberta Canada: ACM; 2002, p. 694–9.
- [26] Vovk V, Petej I. Venn-Abers predictors 2014.
- [27] Vovk V, Gammerman A, Shafer G. *Algorithmic Learning in a Random World*. Cham: Springer International Publishing; 2022.

- [28] Lei J, Wasserman L. Distribution-free Prediction Bands for Non-parametric Regression. *J R Stat Soc Ser B Stat Methodol* 2014;76:71–96.
- [29] Papadopoulos H, Proedrou K, Vovk V, Gammerman A. Inductive Confidence Machines for Regression. In: Elomaa T, Mannila H, Toivonen H, editors. *Mach. Learn. ECML 2002*, vol. 2430, Berlin, Heidelberg: Springer Berlin Heidelberg; 2002, p. 345–56.
- [30] Toccaceli P, Nouretdinov I, Gammerman A. Conformal Predictors for Compound Activity Prediction. In: Gammerman A, Luo Z, Vega J, Vovk V, editors. *Conform. Probabilistic Predict. Appl.*, vol. 9653, Cham: Springer International Publishing; 2016, p. 51–66.
- [31] Fontana M, Zeni G, Vantini S. Conformal Prediction: a Unified Review of Theory and New Challenges. *Bernoulli* 2023;29.
- [32] Vazquez J, Facelli JC. Conformal Prediction in Clinical Medical Sciences. *J Healthc Inform Res* 2022;6:241–52.
- [33] Nixon J, Dusenberry M, Jerfel G, Nguyen T, Liu J, Zhang L, et al. Measuring Calibration in Deep Learning 2020.
- [34] Christodoulou E, Ma J, Collins GS, Steyerberg EW, Verbakel JY, Van Calster B. A systematic review shows no performance benefit of machine learning over logistic regression for clinical prediction models. *J Clin Epidemiol* 2019;110:12–22.
- [35] Niculescu-Mizil A, Caruana R. Predicting good probabilities with supervised learning. *Proc. 22nd Int. Conf. Mach. Learn. - ICML 05*, Bonn, Germany: ACM Press; 2005, p. 625–32.
- [36] Bai Y, Mei S, Wang H, Xiong C. Don't Just Blame Over-parametrization for Over-confidence: Theoretical Analysis of Calibration in Binary Classification 2021.
- [37] De Hond AAH, Kant IMJ, Honkoop PJ, Smith AD, Steyerberg EW, Sont JK. Machine learning did not beat logistic regression in time series prediction for severe asthma exacerbations. *Sci Rep* 2022;12:20363.
- [38] Park JE, Park SY, Kim HJ, Kim HS. Reproducibility and Generalizability in Radiomics Modeling: Possible Strategies in Radiologic and Statistical Perspectives. *Korean J Radiol* 2019;20:1124.
- [39] Guo C, Pleiss G, Sun Y, Weinberger KQ. On Calibration of Modern Neural Networks 2017.
- [40] Austin DE, Lee DS, Wang CX, Ma S, Wang X, Porter J, et al. Comparison of machine learning and the regression-based EHMRG model for predicting early mortality in acute heart failure. *Int J Cardiol* 2022;365:78–84.
- [41] Christodoulou E, Ma J, Collins GS, Steyerberg EW, Verbakel JY, Van Calster B. A systematic review shows no performance benefit of machine learning over logistic regression for clinical prediction models. *J Clin Epidemiol* 2019;110:12–22.

## Supplementary material

This supplementary material details the hyperparameter tuning process and model selection strategy employed in our study. We utilized a 3-fold cross-validation (CV) approach combined with a grid search to optimize hyperparameters for each model. The specific hyperparameters explored for each model, along with their corresponding values, are listed in Supplementary Table 1. Hyperparameters not listed were left at their default values as implemented in the respective libraries.

**Supplementary table 1:** Hyperparameters used in this study. Hyperparameters not listed were left at their default values.

Model	Library	Hyperparameters	Values
Logistic Regression	scikit-learn	penalty	l2, l1
		C	1, 0.1, 10, 100, 0.01
		solver	liblinear
		class_weight	balanced
		max_iter	2000
Random Forest	scikit-learn	n_estimators	5, 20, 50
		min_samples_leaf	2, 4
		min_samples_split	2, 4
		class_weight	balanced
Support Vector Machine (SVM)	scikit-learn	C	1, 0.1, 10, 0.01
		kernel	rbf
		gamma	scale
		class_weight	balanced
		probability	TRUE
XGBoost	xgboost	n_estimators	5, 20, 50
		learning_rate	0.1, 0.01
		subsample	0.5, 1
		scale_pos_weight	Calculated based on class distribution for each fold